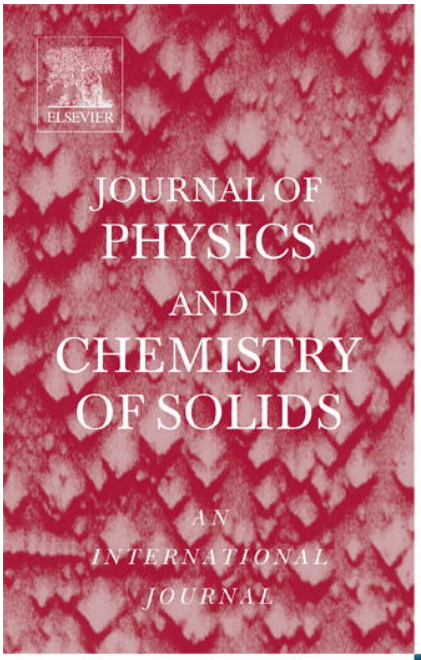

VOLUME 68 No. 7 ISSN 0022-3697
2007 JULY

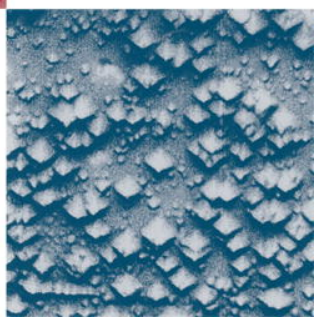

Available online at www.sciencedirect.com
ScienceDirect
Journal of Physics and Chemistry of Solids 68 (2007) 1315–1323
JOURNAL OF PHYSICS AND CHEMISTRY OF SOLIDS
www.elsevier.com/locate/jpcs

Electron paramagnetic resonance and positron annihilation study of the compensation mechanisms in donor-doped $BaTiO_3$ ceramics

Miriam S. Castro[a,*], Walter Salgueiro[b], Alberto Somoza[b,c]

[a]Instituto de Investigaciones en Ciencia y Tecnología de Materiales (INTEMA), Universidad Nacional de Mar del Plata and Consejo Nacional de Investigaciones Científicas y Técnicas (CONICET), J. B. Justo 4302, B7608FDQ Mar del Plata, Argentina
[b]Instituto de Física de Materiales Tandil (IFIMAT), Universidad Nacional del Centro de la Provincia de Buenos Aires, Pinto 399, B7000GHG Tandil, Argentina
[c]Comisión de Investigaciones Científicas de la Provincia de Buenos Aires, Argentina

Received 10 July 2006; received in revised form 7 February 2007; accepted 9 February 2007

Abstract

A study of the defect structure of $BaTiO_3$-based ceramics and their correlation with the compensation mechanisms is presented. The addition of different Nb_2O_5, Sb_2O_3 or La_2O_3 oxide contents (ranging from 0.05 to 0.60 mol%) to commercial $BaTiO_3$ powders allowed to obtain the sintered specimens. EPR spectroscopy was used to characterize the paramagnetic species in the crushed samples. Information regarding bulk and vacancy-like defects in the studied specimens was also obtained using positron annihilation lifetime spectroscopy. Also, complementary analysis through tetragonality parameters and measurements on the real permittivity were carried out. The obtained results show a dependence of the defect profile of the $BaTiO_3$-based specimens on the concentration and type of additive. For high additive content samples, titanium point-like defects were detected; while barium vacancies were detected in samples with low antimony content. Furthermore, oxygen vacancies were revealed in samples with low lanthanum addition. A relationship among the doping level and defect structure is proposed.

Keywords: A. Electronic materials; C. Positron annihilation spectroscopy; D. Electron paramagnetic resonance (EPR); D. Defects

1. Introduction

Barium titanate ceramic is a well-known ferroelectric ceramic that has been of practical importance for about 50 years because of its excellent dielectric properties. When donor doped $BaTiO_3$ ceramics is introduced, the material gets n-type semiconductor characteristics and exhibits a positive temperature coefficient of resistivity (PTCR). Intergranular barrier layers at the grain boundaries govern the electrical properties in $BaTiO_3$-based ceramics [1]. It has been observed that after addition of 0.3 mol% of Nb_2O_5, La_2O_3, Sb_2O_3 or MnO_2 among others, insulating $BaTiO_3$ becomes semiconductor [1]. Higher donor oxide concentration inhibits grain growth and reverts the semiconductor behavior to insulator [2–4]. Reported studies suggest that changes in the electrical behavior and grain growth inhibition phenomena are ruled by a change in the charge compensation mechanism on dopant incorporation [5]. For this reason, with the aim to optimize the electrical behavior is necessary to know and to control the compensation mechanisms operating in barium titanate.

Electron paramagnetic resonance spectroscopy (EPR) is a powerful tool in identifying impurities defects with unpaired electrons. The high sensitivity of EPR allows to detect paramagnetic defects present with low concentrations. This technique was employed by several authors to identify paramagnetic vacancies in $BaTiO_3$ [6–9]. Unfortunately, not only paramagnetic defects exist in the samples therefore EPR only gives partial information about the vacancies concentration.

Positron annihilation spectroscopy (PAS) is a well-established high-sensitivity technique for detecting open

*Corresponding author. Fax: +54 223 4810046.
E-mail address: mcastro@fi.mdp.edu.ar (M.S. Castro).

0022-3697/$ - see front matter © 2007 Elsevier Ltd. All rights reserved.
doi:10.1016/j.jpcs.2007.02.017

volume sites, i.e. vacancy-like defects, in solids. It also has a high sensitivity for the chemical environment of this species of lattice defects (for general information, see [10,11]). It has been applied to the study of the defect structure in solids since almost 30 years, and is presently used in many fields of materials science, from building materials (for instance, cement and polymers to semiconductor-based systems for the information technology). In comparison with imaging and diffraction techniques, it has the advantage of being non-destructive.

PAS studies on perovskites materials were recently laid. For instance, two authors of the present work reported results on thermal equilibrium measurements on $BaTiO_3$ single crystals using positron annihilation lifetime spectroscopy (PALS) technique [12]. The explored temperature range included the ferroelectric to paraelectric phase transition. In this paper, modifications of the charge state of non-equilibrium vacancies occurring at moderate temperature and microstructural changes taking place at high temperature were also suggested. Previous information regarding positron annihilation studies in $BaTiO_3$ can be found in the paper mentioned and references therein [12]. The Halle's group [13,14] reported studies on defects in polycrystalline donor doped $BaTiO_3$ samples. On the other hand, *ab initio* calculations of the positron lifetime for free and defect-trapped positrons were reported by Ghosh et al. [15]. Also, a preliminary study of barium titanate through PAS and EPR was recently reported [16].

The present work relates the stabilized defect profile with the additive oxide and its concentration. Furthermore, a detailed study on the vacancy-type defects allowed us to propose consistent incorporation reactions.

2. Experimental

Base materials were prepared from technically pure $BaTiO_3$ powder (TAM Ceramics Inc., impurity levels: $SrO = 150$ ppm, $CaO < 20$ ppm, $Fe_2O_3 < 70$ ppm, $SiO_2 < 75$ ppm, $Al_2O_3 < 75$ ppm, Mn as a minor impurity, particle size 0.84 μm, Ba/Ti 1.000). Samples were prepared with $BaTiO_3$ particles doped with 0.05, 0.15, 0.30 or 0.60 mol% of analytical grade La_2O_3 (Anedra), Nb_2O_5 (Fluka A.G., Buchs S.G.) or Sb_2O_3 (Aldrich). Raw materials were mixed in the alcoholic medium for 5 min with a high-speed turbine. Slurries were dried at 65 °C. Mixtures were crushed into powders and sieved through a 100 μm mesh screen. Powders were isostatically pressed at 200 MPa and sintered in air at 1350 °C for 2 h or at 1400 °C for 2 or 4 h, with a heating/cooling rate of 3 °C/min.

Scanning electron microscopy (SEM) (Philips 505) was used to reveal and analyze microstructures on fractured, polished and thermally etched samples of $BaTiO_3$-doped ceramics. X-ray diffraction analysis (XRD) were carried out on thermally treated and sintered samples using a Philips 1830 equipment running with CuKα radiation. In order to avoid a possible overlapping of the reflections of the (2 0 0) and (0 0 2) planes in samples with very low tetragonality, the tetragonality parameter (c/a) was calculated from the reflections of (1 1 1) and (2 0 0) planes of sintered $BaTiO_3$. A scanning rate of 0.125 °/min was used.

To characterize the paramagnetic species in the crushed samples at room temperature (*RT*), a Bruker ER-200D (Band X) EPR spectroscope with a gain of 2×10^4, a power of 5 dB and modulation amplitude of 6.3 Gpp was used. The EPR signal intensities were labeled as double integrated intensities (DII) calculated from the empirical relation reported by Murugaraj et al. [6]

$$\mathrm{DII} = [(\text{signal height}) * (\text{signal width})^2]/[(\text{gain}) * (\text{sample mass}) * (\text{modulation amplitude}) * (\text{power})^{1/2}]. \quad (1)$$

PALS spectra were taken at *RT* with a standard fast–fast time spectrometer having a high counting rate (coincidence rate: ~500 counts/s; prompt FWHM: 250 ps). A 20 μCi source of $^{22}NaCl$ deposited on a thin Kapton foil was sandwiched between two identical specimens. Typical runs of 60 min were taken. The source contribution and the response function were evaluated by means of the RESOLUTION code [17]. The lifetime spectra were deconvoluted through the POSITRONFIT program [17]. After subtraction of the source component, the spectra were analyzed as a single exponential lifetime component. For more experimental details see [18,19]. The lifetime τ obtained is an effective parameter associated with this type of data treatment. From the statistical viewpoint, it is a very reliable parameter of the spectra. Furthermore, changes in the average positron lifetime higher than 1 ps are representative of true microstructural modifications of the studied materials.

Electrical properties were measured on silver-palladium coated discs. The real part of the dielectric permittivity versus temperature curves were recorded in the temperature range from 20 to 140 °C with a Hewlett Packard LCR meter 4284A at a frequency of 1 kHz and a voltage of 1 V.

3. Results and discussion

3.1. EPR measurements

Apart from the Mn^{2+} sextet [20] due to the common Mn impurity in $BaTiO_3$ powders, the EPR analysis revealed two singlets states with variable intensity at $g = 2.004$ and $g = 1.973$ in samples with Nb_2O_5, Sb_2O_3 or La_2O_3 addition. The EPR signal from Mn^{2+} depends on the dopant site preference, the dopant content, the particle size [20] and the Ba/Ti ratio [21]. In the $BaTiO_3$ lattice Mn^{2+} substitutes the Ti^{4+} ion within an octahedron formed by six O^{2-}. This paramagnetic ion is very sensitive to the symmetry changes which occur at the Ti^{4+} site for all the structural transmutations [20]. As an example, Fig. 1 shows EPR spectra corresponding to samples with niobium addition. Hari and Kutty [22] assigned the $g = 1.997$ singlet to barium vacancies and the signal at $g = 1.963$ to

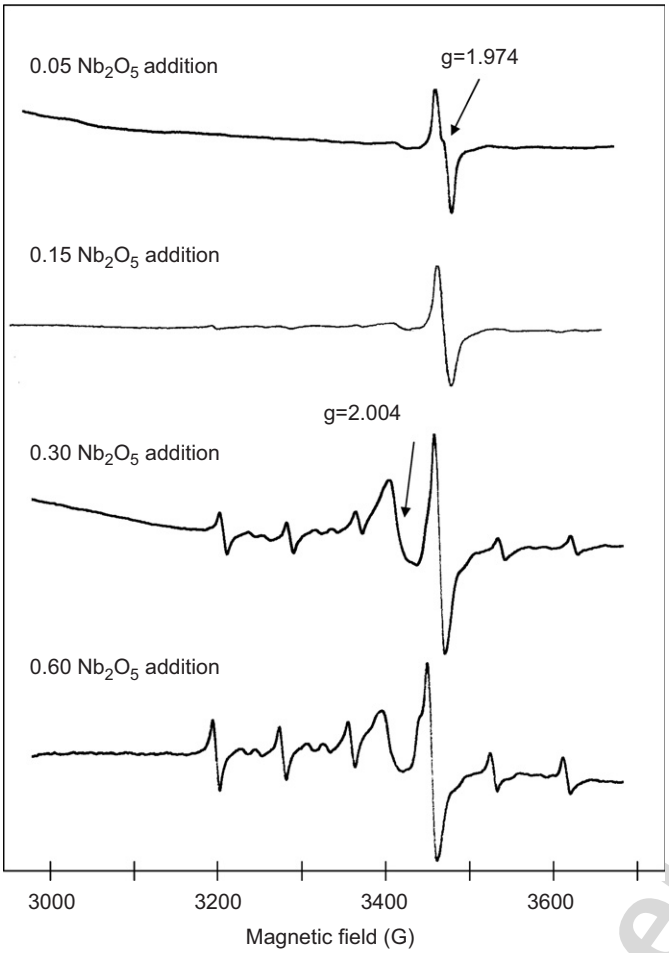

Fig. 1. EPR spectra of samples with niobium addition.

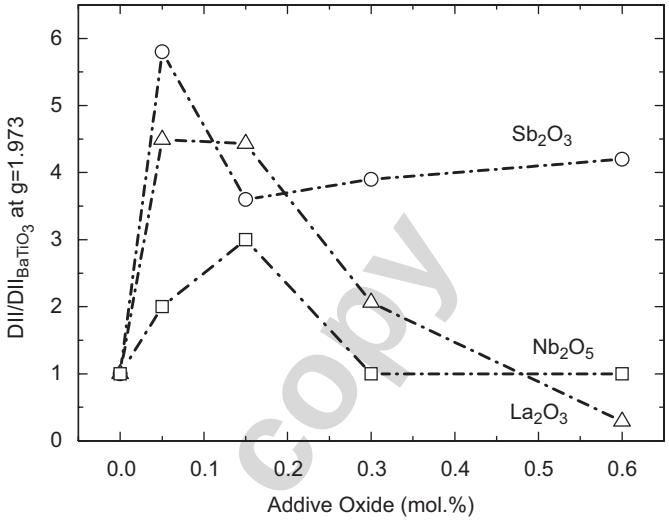

Fig. 2. Relative double-integrated intensity of the EPR-signal at $g = 1.973$ as a function of the additive oxide A_2O_x content (see text). Dash-dot lines are only eye guide.

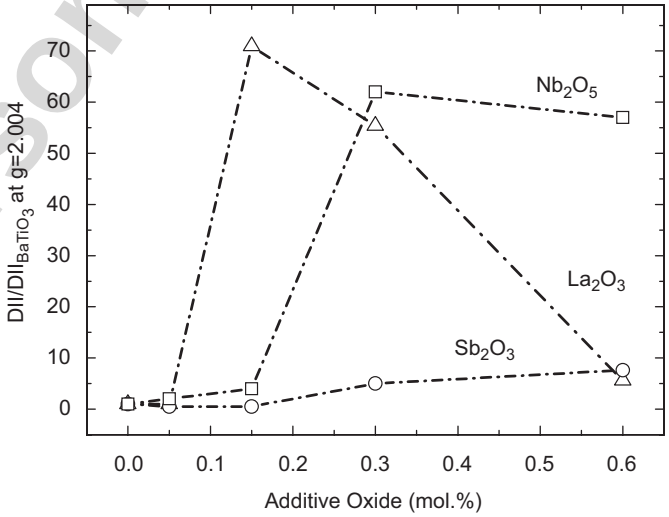

Fig. 3. Relative double-integrated intensity of the EPR-signal at $g = 2.004$ as a function of the additive oxide A_2O_x content (see text). Dash-dot lines are only eye guide.

possibly trapped electrons, resonanting between the oxygen vacancy and two of the adjoining titanium ions [22–24]. Jida et al. [8] assigned the singlet signal at $g = 2.005$ to vacancy-pairs of $V_{Ba}-F^+$ type and the singlet signal at $g = 1.975$ to Cr^{3+} ions due to transition-metal impurities. Glinchuk et al. [25] assigned the EPR signal with $g = 1.963$ to $Ti^{3+}-Ln^{3+}$ (Ln =rare-earth ion). However, Dunbar et al. [26] determined that unlike $Ti^{3+}-Ln^{3+}$ complexes its g value remained constant at 1.974 regardless of lanthanide dopant or concentration. Kolodiazhnyi et al. [7] and Dunbar et al. [26] associated EPR singlets with $g = 2.004$ and 1.973 to intrinsic point defects, V_{Ti} (probably V'_{Ti} or V'''_{Ti}) and V'_{Ba}, respectively. Different authors [7,9] also observed a signal at $g = 1.932$ in n-semiconducting $BaTiO_3$ ceramics, which became negligible on further oxidation. In conclusion, the assignment of EPR signals as reported in the literature is rather controversial.

From Fig. 2, for low additive contents changes in the DII of the EPR-signal at $g = 1.973$ can be inferred. Here, the assignation of $g = 1.975$ to Cr^{3+} was discarded because the signal intensity registered variation with the additive (type or concentration). We will assume that this signal is due to the presence of barium vacancies. On the contrary, from Fig. 3 low changes in the DII of the EPR-signal at $g =$ 2.004 are observed. The possible assignation of the signal at $g = 2$ to Fe^{3+} was discarded because the other resonances ($g = 6.26$, 5.54, 2.47, and 1.62) were not found. In this paper we will employ the defect assignation reported by Kolodiazhnyi et al. [7]. On the other hand, for high Nb_2O_5 and Sb_2O_3 content the number of barium vacancies decreases and that of the titanium vacancies increases. For intermediate La_2O_3 contents an increase of the titanium vacancies can be deduced. For high La_2O_3 concentration a decrease in both barium and titanium paramagnetic vacancies amounts is observed. These assignments will be corroborated below with PALS results.

On the other hand, when the sample with the addition of 0.6 mol% Nb_2O_5 was sintered at 1400 °C for 2 h, an

important diminution in the titanium vacancies concentration was registered ($DII/DII_{BaTiO_3} = 57$ for the sample sintered at 1350 °C for 2 h, $DII/DII_{BaTiO_3} = 22.5$ for the sample sintered at 1400 °C for 2 h). However, the intensity of the signal corresponding to barium vacancies was not modified by the sintering temperature. Moreover, above the 1320 °C threshold (eutectic in the $BaO-TiO_2$ system) secondary phases, in materials highly doped, were registered. Previous studies have reported that a small amount of a glassy phase around the $BaTiO_3$ particles improves the dopant distribution and the particle rearrangement [27]. Besides, liquid fills the grain junctions and removes the porosity on firing. However, sintering at high temperatures for long times could increase the amount of secondary phases deteriorating the final microstructure. Indeed, from SEM analysis a notable increasing in the secondary phase formation was registered.

3.2. Positron lifetime measurements

3.2.1. $BaTiO_3$-based ceramics with different La_2O_3 contents

In Table 1, positron lifetime values obtained measuring specimens of free oxide $BaTiO_3$ and $BaTiO_3$-based ceramics with different lanthanum oxide contents are shown.

The positron lifetime measured for the ceramic with the addition of the lowest oxide content is lower than that corresponding to the undoped ceramic. A further increase in the addition of oxides until 0.30 mol% La_2O_3 induces a strong monotonic increase in τ. For a higher additive content this parameter remains constant, within the experimental scatter.

In order to discuss the PALS data presented in Table 1, the different results published on this kind of $BaTiO_3$-based ceramics must be taken into account. Thus, Macchi et al. reported the positron lifetime in well-annealed $BaTiO_3$ single crystal $\tau_b^{BaTiO_3} = 166 \pm 1$ ps [12]. While the theoretical lifetime prediction reported for free annihilation in bulk $BaTiO_3$ is equal to 152 ps [15], measuring at *RT* and after annealing in air at atmospheric pressure a lifetime ~175 ps was reported for sintered $BaTiO_3$ [13,14]. On the other hand, oxygen vacancies are believed to be effective positron traps in other perovskites [28,29]. The effect of oxygen vacancies, possibly in the form of complexes with metal ion vacancies, is also strongly supported by the results reported by Massoud et al. [13] and Mohsen et al. [14]. However, there are no experimental values reported regarding the positron lifetimes for O-, Ba-, and Ti-vacancies. From the literature, only those predicted by *ab initio* calculations are available, i.e. $\tau_v^O = 162$ ps, $\tau_v^{Ba} = 293$ ps and $\tau_v^{Ti} = 204$ ps, respectively, [15].

Taking in mind the above-mentioned issues, despite the sintered $BaTiO_3$ does not have extra additive elements the positron lifetime obtained measuring the undoped specimens ($\tau_f^{BaTiO_3} \sim 187$ ps) would indicate that some structural defects are present in the studied specimens. Despite the existence of oxygen vacancies cannot be discarded, the low lifetime associated with this kind of defects could not allow to explain the measured τ value. The disagreement with previously reported lifetime values for sintered titanate barium samples [13,14] can be assigned to the fabrication procedure.

With the addition of a very low concentration of Lanthanum oxides, the initial lifetime decrease would indicate positron annihilation mainly in: (a) structural defects of the basic ceramic mentioned above and (b) oxygen vacancies. Considering that positron annihilation in oxygen vacancies gives a lower lifetime than that measured for undoped barium titanate ($\tau_v^O = 162$ ps $< \tau_f^{BaTiO_3} \sim 187$ ps), this last annihilation process in vacancy-type defects is the only one way to contribute to a decrease in τ. For higher additive concentrations ranged from 0.15% to 0.6% La_2O_3 the important lifetime increase in comparison to undoped $BaTiO_3$ ceramic strongly indicates positron annihilation in titanium vacancies. This assumption is also supported for EPR results shown in Fig. 3 which allow us to discard positron annihilation in barium vacancies.

On the other hand, it is well-known that Ti-vacancies have direct influence on the grain growth [30]. In such a way, Mohsen et al. [14] reported positron annihilation in grain boundaries in the same materials. In agreement with this paper and as will be demonstrated below, in the present work, the role of grain boundaries as possible positron trapping sites must be taken into account for high additive content samples.

In Table 1 the average grain size of the sintered samples are also reported. The values reported were estimated using SEM. From these results, a notable grain growth inhibition with lanthanum addition is observed.

To analyze the possible contribution of the grain boundaries to the positron signal in the studied ceramics, we have used previously studied reports by one of the authors of the present work on the process of positron trapping at grain boundaries [31, 32]. In such works the authors reported that for grain sizes higher than about

Table 1
Positron lifetime measured on samples of $BaTiO_3$ and $BaTiO_3$-based ceramics with different Lanthanum additive (La_2O_3 oxides) contents (in mol%)

Sample	$BaTiO_3$	$99.95\%BaTiO_3 + 0.05\%La_2O_3$	$99.85\%BaTiO_3 + 0.15\%La_2O_3$	$99.7\%BaTiO_3 + 0.3\%La_2O_3$	$99.4\%BaTiO_3 + 0.6\%La_2O_3$
Lifetime (ps)	187.0 ± 0.5	183.8 ± 0.6	190.5 ± 0.4	196.2 ± 0.7	196.7 ± 0.7
Grain size (μm)	107	3.5	1.9	1.2	0.72

In the last row of this table the average grain size of the different ceramics studied are also reported.

3 μm positron trapping gives no appreciable signal to positron lifetime spectra. Therefore, only the specimens containing $\geqslant 0.3$ mol% of this type of oxide could contribute to the positron lifetime.

As a conclusion, for high La_2O_3 concentration positron trapping is dominated by Ti vacancies and grain boundaries as well. Positron annihilation in oxygen vacancies cannot be discarded but considering the absolute values of the positron lifetime measured in this work, if there exists, should be negligible.

3.2.2. *Influence of additives in* $BaTiO_3$*-based ceramics on the positron lifetimes*

From previous studies, in 99.95% $BaTiO_3$ − 0.05% Nb_2O_5 (mol%) an abnormal grain growth was observed revealing grains with sizes ~100 μm together with others with typical sizes of 10 μm [33]. This behavior is the typical one observed in the undoped barium titanate. However, when the foreign oxide content of the ceramic is around 0.6% Nb_2O_5, typical grain sizes are around 1 μm [33]. In the case of Sb-contenting oxides, for the lowest oxide content grain sizes between 5 and 20 μm were revealed; while ~1 μm was the typical grain size measured in specimens containing 0.6% Sb_2O_3 [34].

In Table 2, positron lifetime values measured on different $BaTiO_3$-based ceramics containing the lowest and the highest additive contents are shown. For comparison, in the table mentioned the lifetime measured on undoped $BaTiO_3$ ceramic is also included.

For low additive concentration of niobium no lifetime changes, within the experimental scatter, are observed. In the case of antimony, an increase in the positron lifetime was measured. In this case, on the base of EPR results and considering the calculated positron lifetimes in vacancy-like defects, this slight increment would indicate a relative increase of the positron trapping, and a further annihilation, in barium vacancies. A detailed discussion about the processes mentioned will be given below.

In the case of high additive concentration of niobium, the strongest lifetime increase in comparison to undoped $BaTiO_3$ ceramic is observed. To explain this behavior, necessarily positrons must be annihilated in titanium vacancies and grain boundaries. Positron trapping in Ba vacancies, either in the ceramic itself or generated by the Nb presence, cannot be discarded. On the other hand, a high addition of Sb oxide causes an important decrease of the positron lifetime in comparison to undoped $BaTiO_3$ ceramic, so positron trapping in oxygen vacancies seems to be a very reasonable mechanism to compete with that corresponding to positron annihilation in the bulk of the ceramic.

Table 2
Positron lifetime (in ps) in $BaTiO_3$ and $BaTiO_3$-based ceramics with different additives (X oxides) and additive contents (in mol%)

Additive	$BaTiO_3$	99.95% $BaTiO_3$ + 0.05%X	99.4% $BaTiO_3$ + 0.6%X
None	187.0 ± 0.5	—	—
La_2O_3		183.8 ± 0.6	196.7 ± 0.7
Nb_2O_5		187.0 ± 0.7	207.2 ± 0.8
Sb_2O_3		189.2 ± 0.5	181.9 ± 0.5

3.3. *Dielectric behavior*

3.3.1. *Influence of the additives*

In Fig. 4 the evolution of the real part of the permittivity (ε') as a function of the temperature obtained by measuring $BaTiO_3$ samples doped with Nb_2O_5 (curves A), Sb_2O_3 (curves B), or La_2O_3 (curves C) is presented. Specifically, these curves were obtained for samples sintered at 1350 °C for 2 h. For sake of clarity, only the two extremes of oxide addition were selected; i.e.: (I) samples doped with 0.05 mol% of the additive; (II) samples doped with 0.60 mol% of the additive. For all slightly doped samples a typical Curie–Weiss response was registered. On the other hand, for highly niobium or antimony doping, the ε' vs. temperature curves exhibit two contributions due to a core–shell structure with chemical and structural gradients across the grains. Samples with a high content of La_2O_3 present a notable diminution in the real permittivity due to the low density of these samples.

3.3.2. *Influence of the sintering treatment*

In Fig. 5 the evolution of the real part of the permittivity as a function of the temperature obtained measuring samples with a 0.6 mol% Nb_2O_5 addition and sintered under different treatments is presented. From these curves, the contribution of the core-shell structure in all the samples is revealed. Besides, it can be seen that the sample sintered at the higher temperature for the longer time shows a wide peak close to the Curie temperature. This behavior could be related to a more important contribution of the shell region than the core one.

3.4. *Tetragonality parameters*

In Table 3 the tetragonality parameter measured on the samples containing the different additives is reported. With the additives incorporation, a significant decrease of the spontaneous strain of the $BaTiO_3$ tetragonal lattice was observed. Samples with high additive content were stabilized in a pseudocubic structure. The non-typical behavior observed for the sample with 0.05 mol% Sb_2O_3 is due to the possible stabilization of Sb^{3+} or Sb^{5+} in the $BaTiO_3$ lattice.

It has been reported [35] that samples with La_2O_3 present a lower dopant incorporation indicating that at 1350 °C the solid solubility limit of La in $BaTiO_3$ is lower than 0.6 mol% and a certain amount of unincorporated La is segregated along the grain boundaries. Lin and Lu [36] studied the solid state reactions between the excess TiO_2, La_2O_3 and $BaTiO_3$. These authors reported the formation of $La_2Ti_2O_7$ which mitigates the donor-doping effect in the

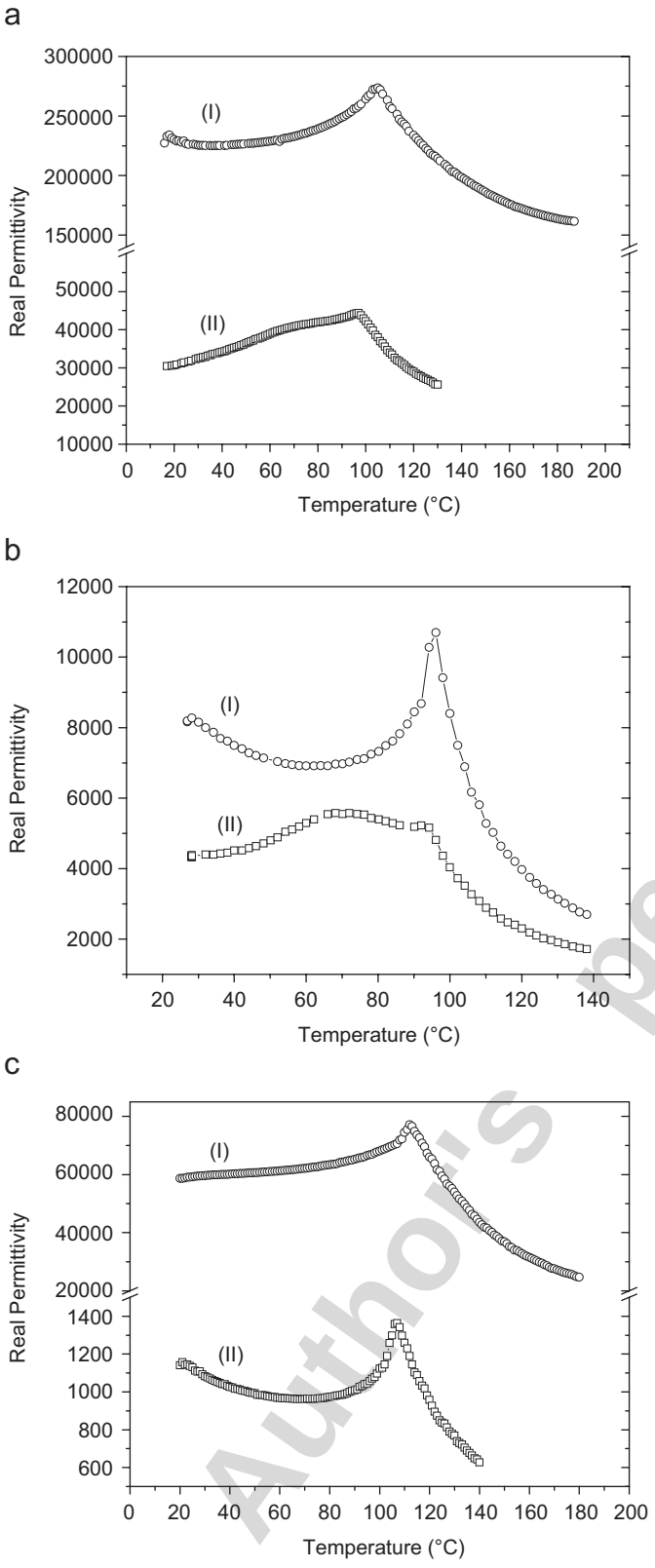

Fig. 4. Real permittivity vs. temperature curves for samples sintered at 1350 °C for 2 h and doped with Nb_2O_5 (a); Sb_2O_3 (b) or La_2O_3 (c). (I) samples doped with 0.05 mol% of the additive; (II) samples doped with 0.60 mol% of the additive.

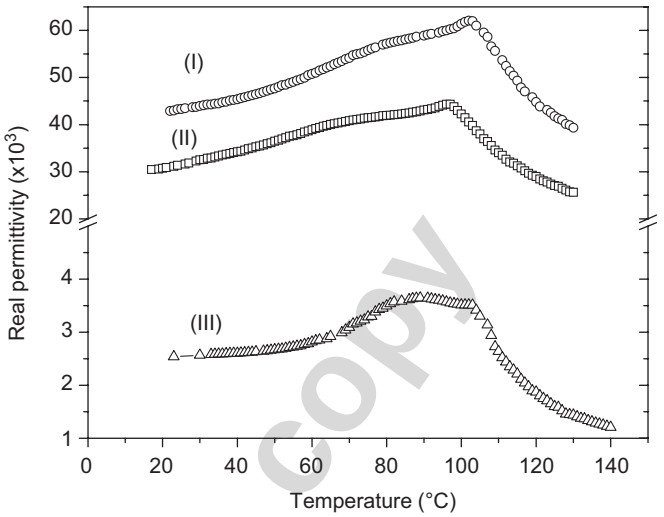

Fig. 5. Real permittivity vs. temperature curves for samples doped with 0.60 mol% Nb_2O_5 and sintered at 1350 °C for 2 h (I); 1400 °C for 2 h (II); 1400 °C for 4 h (III).

Table 3
Tetragonality parameter (c/a) of $BaTiO_3$ and $BaTiO_3$-based ceramics with different additives (X oxides) and additive contents (in mol%)

Additive	$BaTiO_3$	99.95%$BaTiO_3$ + 0.05%X	99.4%$BaTiO_3$ + 0.6%X
None	1.012	—	—
La_2O_3		1.012	1.008
Nb_2O_5		1.010	1.003
Sb_2O_3		1.014	1.004

solid-solution defect regime, particularly in the initial stage of sintering.

3.5. Compensation mechanisms

3.5.1. Samples with low additive content

From PALS and EPR results, samples with low additive content did not show an increase in the titanium vacancies concentration. From PALS results, the variation in the paramagnetic barium vacancies concentration detected by EPR only can be attributed to the formation of new barium vacancies in samples with antimony addition. The presence of oxygen vacancies in samples with lanthanum addition is supported by PALS results. Furthermore, in these samples, the electronic compensation is a relevant mechanism.

The most probable compensation mechanisms are detailed in the following equations:

Nb_2O_5 addition:

From PALS and EPR results electronic compensation is the most favorable mechanism

$$Nb_2O_5 + 2Ti_{Ti} \rightarrow 2Nb_{Ti}^{\cdot} + 2TiO_2 + 2e' + \tfrac{1}{2}O_2. \quad (2)$$

In these samples, the increase in the paramagnetic barium vacancies detected through EPR could be attrib-

uted to the transformation of neutral paramagnetic defects ($V^{x}_{Ba} + e' \rightarrow V'_{Ba}$). The presence of new barium vacancies cannot be justified from PALS results.

Sb_2O_3 addition:

At low additive content, electronic compensation without new defects formation should be considered as

$$Sb_2O_3 + 2Ba_{Ba} \rightarrow 2Sb_{Ba}^{\cdot} + 2BaO + 2e' + \tfrac{1}{2}O_2. \quad (3)$$

In this case, stabilization of Sb^{5+} must not be neglected

$$Sb_2O_5 + 2Ti_{Ti} \rightarrow 2Sb_{Ti}^{\cdot} + 2TiO_2 + 2e' + \tfrac{1}{2}O_2. \quad (4)$$

Also, according to EPR and PALS results, the barium vacancies formation must be also considered

$$Sb_2O_3 + 2Ba_{Ba} \rightarrow 2Sb_{Ba}^{\cdot} + V''_{Ba} + 3BaO, \quad (5)$$

$$Sb_2O_5 + 2\,Ti_{Ti} + Ba_{Ba} \rightarrow 2Sb_{Ti}^{\cdot} + V''_{Ba} + TiO_2 + BaTiO_3. \quad (6)$$

La_2O_3 addition:

For low lanthanum addition, substitution at the barium site with electronic compensation must be considered [25]

$$La_2O_3 + 2Ba_{Ba} \rightarrow 2La_{Ba}^{\cdot} + 2BaO + 2e' + \tfrac{1}{2}O_2. \quad (7)$$

The decreasing in the positron lifetime discussed in Section 3.2 was attributed to the possible formation of oxygen vacancies. Due to the large difference in the ionic radii of La^{3+} and Ti^{4+}, the following compensation mechanism is improbable

$$La_2O_3 + 2Ti_{Ti} + O_o \rightarrow 2La'_{Ti} + V^{\cdot\cdot}_{O} + 2TiO_2. \quad (8)$$

Therefore, oxygen vacancies could be produced by oxygen loss during the sintering process, as it was proposed by Morrison et al. [37] or by the influence of acceptor impurities following the compensation equation:

$$MnO + Ti_{Ti} + O_o \rightarrow Mn''_{Ti} + V^{\cdot\cdot}_{O} + TiO_2. \quad (9)$$

Through EPR the signal corresponding to paramagnetic oxygen vacancies was not detected and the signal corresponding to paramagnetic barium vacancies could be attributed to the transformation of neutral to paramagnetic defects ($V^{x}_{Ba} + e' \rightarrow V'_{Ba}$).

3.5.2. Samples with high additive content

For higher doping level, according to PALS and EPR results, the presence of titanium vacancies prevails in samples with niobium or lanthanum addition. However, in samples with antimony addition, oxygen vacancies formation can not be discarded. For these samples, the most probable compensation mechanisms are detailed as follows:

Nb_2O_5 addition:

For niobium addition, EPR results indicate a notable increasing in the titanium vacancies. Also, PALS results were correlated with the presence of titanium vacancies and an important presence of grain boundaries. In this case, both techniques show similar information and the most probable compensation equation is the following one:

$$2Nb_2O_5 + 5Ti_{Ti} \rightarrow 4Nb_{Ti}^{\cdot} + V''''_{Ti} + 5TiO_2. \quad (10)$$

Using SEM and EDS analysis the presence of a secondary phase with a composition close to $Ba_6Ti_{17}O_{40}$ was reported [33]. This secondary phase would contain the TiO_2 expelled during the niobium incorporation.

Sb_2O_3 addition:

For high level of antimony addition, EPR results indicate the presence of barium and titanium vacancies. However, from PALS results the positron lifetime decrease could be related to the formation of oxygen vacancies and a very little amount of titanium vacancies. Therefore, it is probable that the changes in the barium vacancies concentration detected by EPR are due to the diamagnetic–paramagnetic transformation. Then, the most probable compensation mechanisms could be

$$2Sb_2O_3 + Ti_{Ti} + 4Ba_{Ba} \rightarrow 4Sb_{Ba}^{\cdot} + V''''_{Ti} + 3BaO + BaTiO_3, \quad (11)$$

$$2Sb_2O_5 + 5Ti_{Ti} \rightarrow 4Sb_{Ti}^{\cdot} + V''''_{Ti} + 5TiO_2, \quad (12)$$

$$Sb_2O_3 + 2Ti_{Ti} + O_o \rightarrow 2Sb'_{Ti} + V^{\cdot\cdot}_{O} + 2TiO_2. \quad (13)$$

Recently, one of the authors of the present paper studied this kind of ceramic with SEM and EDS [34]. From the analysis of the information obtained the presence of a secondary phase with a Ti/Ba ratio near to 2 was reported. This result is in agreement with the mechanisms proposed in Eqs. (12) and (13).

La_2O_3 addition:

For Lanthanum addition, the increasing in the positron lifetime could be related to the formation of titanium vacancies according to the following equation:

$$2La_2O_3 + Ti_{Ti} + 4Ba_{Ba} \rightarrow 4La_{Ba}^{\cdot} + V''''_{Ti} + 3BaO + BaTiO_3 \quad (14)$$

and to a notable increasing in the grain boundaries content. These results are related to the changes in the paramagnetic titanium vacancies concentration detected by EPR for samples with 0.15 mol% of La_2O_3. However, for samples with higher additive concentration PALS and EPR results showed some contradiction. Taking into account that EPR supplies only information about the paramagnetic defects in the sample, the complete characterization of the vacancies present in the samples cannot be extracted from this technique. For this reason, it is more convenient to extract information about the vacancy-type defect state from PALS results.

The BaO expulsion from the $BaTiO_3$ lattice was corroborated by the formation of a barium-rich secondary phase detected by XRD.

In general, at low doping levels the BaO or the TiO_2 expelled could be incorporated in the perovskite lattice (with the formation of cation and oxygen vacancies) changing the Ba/Ti ratio according to the excluded oxide. However, for high additive contents, secondary phases are formed with the expelled oxides [38]. These changes in the Ba/Ti ratio could modify the final additive incorporation into the $BaTiO_3$ lattice [21].

3.6. Corroboration of the EPR-signal assignment

The compensation mechanisms proposed in the present work are a consequence of the experimental information obtained using systematic experimental studies with EPR and PALS techniques jointly. In such a way, it was possible to go deeper in the analysis of the adequate compensation mechanism operating in the different barium titanate ceramics with the addition of A_2O_x oxides proposed in the literature.

On the other hand, details about the EPR assignment signals could be extracted. Some authors claim that g values around 1.997–2.004 and around 1.963–1.973 should be attributed to barium vacancies and oxygen vacancies [22–24], whereas others to V_{Ti} and V_{Ba}, respectively [7,26]. Taking into account the more simple case (i.e. samples with high Nb_2O_5 addition) the extraordinary increasing in the EPR signal at $g = 2.004$, and the fact that the positron lifetime measured is very close to τ_V^{Ti} allow to conclude that the EPR signal must be assigned to titanium vacancies. An increase of the barium vacancies cannot be justified through PALS results. On the other hand, in samples with low antimony addition, the increasing in the lifetime cannot justify the presence of oxygen vacancies and, therefore, the increasing in the signal at $g = 1.973$ should be attributed to barium vacancies.

Also, in heavily doped samples, not all the additive content could be effectively incorporated into the $BaTiO_3$ lattice. Therefore, it could be segregated at the grain boundaries or a concentration gradient of the additive into the grains could be present, as is strongly suggested by the dielectric measurements (Figs. 4 and 5).

The profile above mentioned could induce different compensation mechanisms inside the grains. It was determined an evolution with the doping level from a tetragonal structure split to a pseudocubic structure. This structural modification could influence the EPR signals. Indeed, the Mn^{2+} spectrum is very sensitive to symmetry changes and the spectra corresponding to the tetragonal and cubic structures can be superposed [20].

On the other hand, due to the nature of the PALS technique it cannot provide information on the gradient concentration of an additive into a sample; therefore, into a grain too.

4. Conclusions

The results obtained can be summarized as follows:

(i) Low additive concentration induces electron compensation mechanism. Also, in samples with antimony addition the formation of barium vacancies was registered. In samples with lanthanum addition the presence of oxygen vacancies was detected.
(ii) In samples with high lanthanum or niobium concentration the presence of titanium vacancies was revealed. Grain boundaries in samples with grain size lower than 3 μm also contribute to increase the average positron lifetime.
(iii) From PALS results, the formation of titanium and oxygen vacancies in samples with high antimony addition could be established.
(iv) Changes in the paramagnetic species concentration could induce to mistakes in the compensation mechanism assignment. Taking advantage of the high-sensitivity of PALS technique to open-volume defects, more accurate results regarding this mechanism could be extracted.
(v) PALS technique provides useful information for the correct assignment of defects in these samples.
(vi) The interpretation of the overall results is complicated by the existence of a concentration gradient (core-shell structure) inside the grains of heavily doped ceramics.

Acknowledgments

Walter Salgueiro and Alberto Somoza acknowledge the financial support of the Agencia Nacional de Promoción Científica y Tecnológica. (PID No. 435/2003 and PICT No. 12-14376/2004), Comisión de Investigaciones Científicas de la Provincia de Buenos Aires and Secretaría de Ciencia y Técnica (UNCentro), Argentina. Miriam Castro is grateful to CONICET and Universidad Nacional de Mar del Plata (Argentina) for the financial support provided for this research. Authors specially thank Dr. Eliana Brzozowski for the samples preparation.

References

[1] L. Hozer, Semiconductor Ceramics—Grain Boundary Effects, PWN Polish Scientific Publishers, Warsaw, Poland, 1994, pp. 109–143.
[2] H. Jonker, Some aspects of semi-conducting barium titanate, Solid State Electron. 7 (1964) 895–903.
[3] M. Drofenik, Origin of the grain growth anomaly in donor-doped barium titanate, J. Am. Ceram. Soc. 76 (1993) 123–128.
[4] Z.C. Li, B. Bergman, Electrical properties and ageing characteristics of $BaTiO_3$ ceramics doped by single dopants, J. Eur. Ceram. Soc. 25 (2005) 441–445.
[5] E. Brzozowski, M.S. Castro, Grain growth control in Nb-doped $BaTiO_3$, J. Mater. Process. Technol. 168 (2005) 464–470.
[6] P. Murugaraj, T.R.N. Kutty, M. Subba Rao, Diffuse phase transformations in neodymium-doped $BaTiO_3$ ceramics, J. Mater. Sci. 21 (1986) 3521–3527.
[7] T. Kolodiazhnyi, A. Petric, Analysis of point defects in polycrystalline $BaTiO_3$ by electron paramagnetic resonance, J. Phys. Chem. Solids 64 (2003) 953–966.
[8] S. Jida, T. Mike, Electron paramagnetic resonance of Nb-doped $BaTiO_3$ ceramics with positive temperature coefficient of resistivity, J. Appl. Phys. 80 (1996) 5234–5239.
[9] R. Scharfschwerdt, A. Mazur, O.F. Schimer, H. Hesse, S. Mendricks, Oxygen vacancies in $BaTiO_3$, Phys. Rev. B 54 (1996) 15284–15290.
[10] A. Dupasquier, A.P. Mills Jr. (Eds.), Positron Spectroscopy of Solids, IOS Press, Amsterdam, 1995.
[11] A. Dupasquier, G. Kögel, A. Somoza, Studies of light alloys by positron annihilation techniques, Acta Mater. 52 (2004) 4707–4726.

[12] C. Macchi, A. Somoza, A. Dupasquier, A. López García, M. Castro, Positron trapping in $BaTiO_3$ Perovskite, J. Phys. Condensed Matter 13 (2001) 5717–5722.
[13] A.M. Massoud, R. Krause-Rehberg, H.T. Langhammer, J. Gebauer, M. Mohsen, Defect studies in $BaTiO_3$ ceramics using positron annihilation spectroscopy, Mater. Sci. Forum 363–365 (2001) 144–146.
[14] M. Mohsen, R. Krause-Rehberg, A.M. Massoud, H. Langhammer, Donor-doping effect in $BaTiO_3$ ceramics using positron annihilation spectroscopy, Radiat. Phys. Chem. 68 (2003) 549–552.
[15] V.J. Ghosh, B. Nielsen, T. Friessnegg, Identifying open-volume defects in doped and undoped perovskie-type $LaCoO_3$, $PbTiO_3$ and $BaTiO_3$, Phys. Rev. B 61 (2000) 207–212.
[16] T. Kolodiazhnyi, A. Younker, P. Malysz, P. Mascher, Defect characterization of barium titanate, tantalates and niobates by PAS and ESR, Mater. Sci. Forum 445–446 (2004) 129–131.
[17] P. Kirkegaard, N.J. Pedersen, M. Eldrup, PATFIT-88 Risø Natl. Lab. M-2740 (1989).
[18] A. Somoza, A. Dupasquier, I.J. Polmear, P. Folegati, R. Ferragut, Positron annihilation study of the aging kinetics of AlCu-based alloys Part I: Al–Cu–Mg, Phys. Rev. B 61 (2000) 14454–14463.
[19] C. Macchi, A. Somoza, A. Dupasquier, I.J. Polmear, Secondary precipitation in Al–Zn–Mg–(Ag), Acta Mater. 51 (2003) 5151–5158.
[20] R. Böttcher, C. Klimm, D. Michel, H.-C. Semmelhack, G. Völkel, H.-J. Gläsel, E. Hartmann, Size effect in Mn^{2+} nanopowders observed by electron paramagnetic resonance, Phys. Rev. B 62 (2000) 2085–2095.
[21] Y. Tsur, T.D. Dunbar, C. Randall, Crystal and defect of rare earth cations I $BaTiO_3$, J. Electroceram. 7 (2001) 25–34.
[22] N.S. Hari, T.R.N. Kutty, Effect of secondary-phase segregation on the positive temperature coefficient in resistance characteristics of n-$BaTiO_3$ ceramics, J. Mater. Sci. 33 (1998) 3275–3284.
[23] N.S. Hari, P. Padmini, T.R.N. Kutty, Complex impedance analyses of n-$BaTiO_3$ ceramics showing positive temperature coefficient of resistance, J. Mater. Sci. 8 (1997) 15–22.
[24] T.R.N. Kutty, P. Murugaraj, Phase relations and dielectric properties of BaTiO3 ceramics heavily substituted with neodymium, J. Mater. Sci. 22 (1987) 3652–3664.
[25] M.D. Glinchuk, I.P. Bykov, S.M. Kornienko, V.V. Laguta, A.M. Slipenyuk, A.G. Bilous, O.I. V'yunov, O.Z. Yanchevskii, Influence of impurities on the properties of rare-doped barium-titanate ceramics, J. Mater. Chem. 10 (2000) 941–947.
[26] T.D. Dunbar, W.L. Warren, B.A. Tuttle, C.A. Randall, Y. Tsur, Electron paramagnetic resonance investigations of lanthanide-doped barium titanate: dopant site occupancy, J. Phys. Chem. B 108 (2004) 908–917.
[27] I. Zajc, M. Drofenik, Grain growth and densification in donor-doped $BaTiO_3$, Brit. Ceram. T. 88 (1989) 223–225.
[28] A. Barathi, Y. Hariharan, A.K. Sood, V. Sankara Sastry, M.P. Janawadkar, C.S. Sundar, Positron annihilation study of oxygen vacancies in $Y_1Ba_2Cu_3O_{7-x}$, Europhys. Lett. 6 (1988) 369–374.
[29] R.S. Brusa, R. Grisenti, S. Liu, S. Oss, O. Pilla, A. Zecca, A. Dupasquier, F.A. Matacotta, Inhibition of positron trapping by charge transfer in ceramic superconductors, Physica C 156 (1988) 65–69.
[30] T. Friessnegg, S. Madhukar, B. Nielsen, A.R. Moodenbaugh, S. Aggarval, D.J. Keeble, E.H. Pointdexter, P. Mascher, R. Ramesh, Metal ion and oxygen vacancies in bulk and thin film $La_{1-x}Sr_xCoO_3$, Phys. Rev. B 59 (1999) 13365–13369.
[31] A. Dupasquier, A. Somoza, Positron trapping in fine-grained materials, Mater. Sci. Forum 175–178 (1995) 35–46.
[32] A. Dupasquier, R. Romero, A. Somoza, Positron Trapping at Grain Boundaries, Phys. Rev. B 48 (1993) 9235–9245.
[33] E. Brzozowski, M.S. Castro, Defect profile and electrical properties of Nb_2O_5-doped $BaTiO_3$ materials, J. Mater. Sci. Mat. Electron. 14 (2003) 471–476.
[34] E. Brzozowski, A.C. Caballero, M. Villegas, M.S. Castro, J.F. Fernández, Effect of doping method on microstructural and defect profile of Sb−$BaTiO_3$, J. Eur. Ceram. Soc. 26 (2006) 2327–2336.
[35] N. Kurata, M. Kuwabara, Semiconducting-insulating transition of highly donor-doped barium titanate ceramics, J. Am. Ceram. Soc. 76 (1993) 1605–1608.
[36] M.-H. Lin, H.-Y. Lu, Densification retardation in the sintering of La_2O_3-doped barium titanate ceramic, Mater. Sci. Eng. A 323 (2002) 167–176.
[37] F.D. Morrison, A.M. Coats, D.C. Sinclair, A. West, Charge compensation mechanisms in La-doped $BaTiO_3$, J. Electroceram. 6 (2001) 219–232.
[38] E. Brzozowski, Desarrollo de ceràmicos basados en $BaTiO_3$ para su aplicación en la industria electrónica, PhD thesis, Universidad Nacional de Mar del Plata, Argentina, 2000.